Full Length Article

Preparation and characterization of noble metal modified titanium dioxide hollow spheres – new insights concerning the light trapping efficiency

Tamás Gyulavári[a,b], Kata Kovács[b], Zoltán Kovács[b,c], Enikő Bárdos[a,b], Gábor Kovács[a,b,c,d], Kornélia Baán[b], Klára Magyari[c], Gábor Veréb[a,e,*], Zsolt Pap[a,d,e,*], Klara Hernadi[a,b]

[a] Research Group of Environmental Chemistry, Institute of Chemistry, University of Szeged, Tisza Lajos krt. 103, H-6720 Szeged, Hungary
[b] Department of Applied and Environmental Chemistry, University of Szeged, Rerrich tér 1, H-6720 Szeged, Hungary
[c] Nanostructured Materials and Bio-Nano-Interfaces Center, Interdisciplinary Research Institute on Bio-Nano-Sciences, Babes-Bolyai University, Treboniu Laurian 42, RO-400271 Cluj-Napoca, Romania
[d] Institute of Environmental Science and Technology, University of Szeged, Tisza Lajos krt. 103, H-6720 Szeged, Hungary
[e] Department of Process Engineering, Faculty of Engineering, University of Szeged, Moszkvai krt. 9, H-6725 Szeged, Hungary

ABSTRACT

Titanium dioxide hollow spheres (TiO_2-HSs) were fabricated by applying carbon spheres (CSs) as templates, which were eliminated by calcination. The most suitable TiO_2 was selected and an attempt was made to further increase its photocatalytic activity *via* noble metal (Au and Pt, at 0.25 wt%) deposition. The photocatalytic efficiency was determined by the decomposition of phenol and oxalic acid under both UV-A and visible light irradiation. It was established, that both the unique morphology and the presence of noble metals contributed to the photocatalytic activity gain compared to the solid spherical reference. For the elucidation of the observed phenol degradation performance under UV-A light irradiation, new insights were proposed: within the TiO_2 samples the ratio of HSs with enhanced light trapping properties were demonstrated, and the data was compared to the observed photocatalytic activities and a direct correlation was found.

1. Introduction

A large number of methods have been suggested to remedy the problem of wastewater treatment from which heterogeneous photocatalysis is a suitable candidate to be used as an alternative technique. Titanium dioxide remains to be one of the most appropriate semiconductors for photocatalytic applications due to its apparent beneficial properties (it is photo- and chemically stable, cheap, accessible in considerable amounts); however, its photocatalytic efficiency is unsatisfactory in numerous cases, making the enhancement of it the main scope of numerous publications. There has been tremendous number of attempts to increase the photocatalytic activity and the excitability of TiO_2, for example (i) preparing composites with other semiconductors [1–4], (ii) doping with various elements [5–9], (iii) sensitizing with dyes [10,11], (iv) modifying with noble metals [12–17] and (v) synthesizing TiO_2 with various morphologies [17–21].

Recently, the preparation of hollow structural semiconductors has attracted considerable attention due to their unique chemical, thermal, optical, electrical and optoelectronic properties [22]. Semiconductors possessing such morphology may have enhanced light harvesting capability due to the multiple reflections of incident light within the hollow cavity which can lead to the improved utilization of light source [23,24], yielding more photogenerated charge carriers, resulting in enhanced photocatalytic efficiency of the semiconductor. Based on the publication of Xiang and Zhao, in which methyl blue was applied as model contaminant, the (visible) light harvesting of the titania cannot be increased effectively only by controlling the morphology, but it is possible to enhance it by combining morphology control with noble metal deposition [19]. Accordingly, it is probable that combining morphology control with other photocatalytic activity enhancement techniques (such as noble metal deposition) will be of particular interest.

It is well-known that noble metal deposition (using noble metals as co-catalysts) can increase the photocatalytic activity of titania because of the fast transfer of photogenerated electrons from TiO_2 to noble metal nanoparticles resulting in decreased e^-/h^+ pair recombination and consequently, enhanced charge separation [25,26]. The deposition of noble metals can also enable the production of hydrogen, an alternate green energy source [12,27].

Table 1
Crystal phase compositions, mean diameters, circularities and specific surface areas of the TiO₂-HSs samples.

Sample name	CS purification solvent	Calcination temperature (°C)	Anatase (wt%)	Rutile (wt %)	D_A (nm)	D_R (nm)	Median (nm)	Circularity	Specific surface area ($m^2 \cdot g^{-1}$)
$TiO_2\_no\_HS_{500}^{Ac}$	acetone	500	97	3	35	66.9	1313	0.99	~6
$TiO_2\_HS_{500}^{Ac}$	acetone	500	87	13	26.5	30.1	1198	0.99	~6
$TiO_2\_HS_{800}^{Ac}$	acetone	800	–	100	–	28.3	1129	0.94	~6
$TiO_2\_HS_{500}^{EtOH}$	ethanol	500	96.6	3.4	18.1	20.9	948	0.98	~6
$TiO_2\_HS_{800}^{EtOH}$	ethanol	800	12.5	87.5	35.1	32.4	1122	0.93	~6
$TiO_2\_HS_{500}^{Ac}$-Au	acetone	500	90.01	9.99	22.2	20.5	1635	0.98	~6
$TiO_2\_HS_{500}^{Ac}$-Pt	acetone	500	91.93	8.07	22.9	29	1333	0.98	~6

Although there are some publications in the literature where noble metal-deposited (Au, Ag, Pt, Pd) hollow spherical TiO₂-s were synthesized [17,19,28,29] their numbers are scarce. Thus, in this study these two techniques (morphology control and noble metal deposition) were combined to increase the photocatalytic activity of TiO₂ photocatalysts. The photocatalytic efficiencies were determined by either using the poorly adsorbing phenol, or oxalic acid with good adsorption properties as model contaminants under UV-A and visible light irradiation. The nature of photocatalytic activity gain was described in detail *via* in-depth morpho-structural characterization and photocatalytic degradation tests using reference titania with or without noble metal co-catalysts and/or hollow spherical morphology. Even though there are numerous publications in the literature for the explanation of the photocatalytic enhancement caused by the deposition of noble metals, but in the case of photocatalytic activity gain caused by the unique hollow spherical morphology the enhanced light trapping properties are only implied in these publications to the best of our knowledge. Thus, in this paper an attempt was made to establish connection between the observed photocatalytic activity and the properties of the TiO₂ hollow spheres based on calculations.

2. Experimental

2.1. Materials

For the synthesis of TiO₂-HSs, Ti(IV) butoxide (Sigma-Aldrich; reagent grade; 97%), was applied as precursor. For the fabrication of CS templates ordinary table sugar (sucrose, Magyar Cukor Zrt., Koronás™) – as carbon source –, NaOH (Molar Chemicals; a.r.; 50%), and ultrapure Millipore Milli-Q (MQ) water were used. For their purification either ethanol (Molar Chemicals; 96%) or acetone (Molar Chemicals; 99.96%) were used. For the determination of photocatalytic activities oxalic acid (Sharlau; analytical grade) and phenol (Spektrum 3D; analytical grade) were used as model pollutants. For the deposition of gold and platinum nanoparticles HAuCl₄·4 H₂O (Sigma-Aldrich; 99.9%) and H₂PtCl₆ (Sigma-Aldrich; 99.9%) were applied, respectively. Trisodium citrate (Sigma-Aldrich; > 99%) was utilized to stabilize the growth of the noble metal particles and for their reduction NaBH₄ (Alfa Aesar; 98%) was used.

2.2. Preparation of the carbon sphere templates

The CS templates were synthesized based on our recent publication [30] as follows. In a Teflon®-lined stainless-steel autoclave (V_{total} = 623 mL) 180.7 mL 0.15 M sucrose solution was prepared (V_{fill}/V_{total} = 29%) and the pH was set to 12 using a 2 M NaOH solution. The as-prepared solution was subjected to hydrothermal treatment in a drying oven at 180 °C for 12 h. The CSs were purified from the residual organic contaminants – which form during the synthesis under the applied conditions – by centrifugation using either ethanol or acetone as solvent. During this procedure the CSs were washed in three cycles at the rate of 13,400 rpm for 3 min using 80 mL solvent per 1 g of CSs. Then, the solid product was collected and dried in air at 40 °C, and finally, was ground in an agate mortar.

2.3. Preparation of TiO₂ hollow spheres and the deposition of noble metals

The preparation of the TiO₂ coating was based on the publication of Ao et al. [23]. 0.1 g CS was added to 20 mL absolute ethanol in a beaker under vigorous magnetic stirring, to which 1 mL Ti(IV) butoxide was added dropwise with a constant rate of 1 mL·min⁻¹. Then, the beaker was covered with parafilm to prevent evaporation, and the suspension was stirred for 4 h. After the formation of the coating, the samples were dried, and ultimately the CSs were eliminated by calcination in a *Thermolyne 21,100 type* tube furnace with constant air supply (30 L·h⁻¹) at either 500 or 800 °C for 3 h applying 5 °C·min⁻¹ heating rate, resulting in crystalline TiO₂-HSs.

Subsequently, gold or platinum nanoparticles were deposited onto the surface of TiO₂-HSs at 0.25 wt%. For this, 800 mg of the as-prepared sample was added to 87 mL MQ water, to which 12.5 mL trisodium citrate (c = 0.63·10⁻⁴ M) was added. Then, either 1.6 mL HAuCl₄ · 4 H₂O (c = 2.54·10⁻² M) or 1.3 mL H₂PtCl₆ (c = 3.13·10⁻² M) were added to the system. For the chemical reduction of noble metals 2 mL precooled (T ∼ 0 °C) NaBH₄ (0.15 M) was applied, and the suspension was stirred for 30 min then purified *via* centrifugation 3 times using MQ water. Finally, the samples were dried in air at 40 °C and ground in an agate mortar. The synthesis parameters – applied during the preparation of the samples in this work – were summarized in Table 1. The as-prepared samples were named based on the following: $TiO_2\_HS_y^x z$, where 'HS' stands for hollow spheres, 'x' is the solvent which was used for the purification of the carbon spheres ('Ac' for acetone and 'EtOH' for ethanol), and 'y' is the calcination temperature which was used for both the elimination of carbon spheres and the crystallization of TiO₂, and 'z' is the deposited noble metal.

For the evaluation of photocatalytic activity gain caused by the unique morphology multiple reference TiO₂ samples were fabricated. The synthesis procedure was carried out almost similarly; the only difference was the absence of CSs. In other words, the solid spherical counterparts of those TiO₂-HSs were synthesized, which were used for the evaluation of photocatalytic activities. The naming of these samples was similar compared to the hollow spherical samples, with the addition of 'no' ('$TiO_2\_no\_HS_y^x z$'), which refers to the absence of CSs, thus the solid spherical morphology of the samples.

2.4. Characterization methods and instrumentation

A *Rigaku Miniflex II* type diffractometer was used for the XRD measurements. The following parameters were applied: 30 mA, 40 kV, $\lambda_{CuK\alpha}$ = 0.15406 nm. The 20–40 (2θ°) interval was recorded using 1 (2θ°)·min⁻¹ scan speed. Mean primary crystallite sizes were calculated applying the Scherrer equation [31,32]. The rutile and anatase weight fractions were determined from their corresponding peak areas (27.5 (2θ°) for rutile and 25.3 (2θ°) for anatase, respectively).

The morphology of the samples was analyzed by a *Hitachi S-4700 Type II* scanning electron microscope and a *FEI TECNAI G² 20 X-Twin* type transmission electron microscope. The former was used to examine the general morphology, while the latter to observe the hollow structure and the presence of noble metals on the surface of the TiO₂

samples. The recorded micrographs were utilized to determine the diameter and calculate the circularity degree [33] of the spheres using the ImageJ software. During SEM measurements the electron beam was produced using a cold field emission gun applying 10 kV acceleration voltage, while in the case of TEM 100 kV was set. The circularity (C) of the spheres was calculated based on the following equation:

$$C = \frac{4\pi A}{P^2}$$

where A is the area and P is the perimeter of the projection of the spheres [33].

The diffuse reflectance (λ = 220–800 nm region) of the samples was studied by a *Jasco-V650* spectrophotometer, equipped with an *ILV-724-type* integration sphere. The band gap energies were evaluated from the derivative spectra of the samples.

The surface of the TiO_2 samples was studied by FT-IR measurements using a *Jasco 6000* spectrometer. The 400–4000 cm^{-1} range was recorded applying 4 cm^{-1} spectral resolution.

The specific surface areas of the TiO_2 samples were determined with a *BELCAT-A* device *via* N_2 adsorption at 77 K using the BET method.

2.5. Evaluation of the photocatalytic efficiencies

The photocatalytic activities were evaluated by the photocatalytic decomposition of phenol ($c_{0,phenol}$ = 0.1 mM) and oxalic acid ($c_{0,oxalic\ acid}$ = 1 mM) both under UV-A (λ_{max} = 365 nm) and visible light irradiation (λ > 400 nm). For the visible light experiments 4 conventional energy-saving lamps (*Düwi 25920/R7S*-24 W), while for the UV experiments 6 fluorescent tubes (*Vilber-Lourmat T-6L UV-A*, 6 W) were applied. The emission spectra of the applied lamps can be seen in Fig. S1. The TiO_2 suspensions were added to a glass vessel which was placed on a magnetic stirrer. During the visible light illumination 1 M $NaNO_2$ solution was circulated in the thermostating jacket of the glass vessel, to cut off UV photons. Constant temperature (25 °C) was assured during the experiments *via* the $NaNO_2$ solution (Vis) or water (UV) using an ultrathermostat. Constant dissolved oxygen level was maintained by supplying air into the photoreactor during the 4-hour-long measurements. The concentration of phenol and oxalic acid was measured with high performance liquid chromatography (HPLC) and the device consisted of a *Merck Hitachi L-7100* low-pressure gradient pump equipped with a *Merck-Hitachi L-4250* UV–Vis detector. For phenol as eluent 50–50% methanol/water mixture ($\lambda_{detection}$ = 210 nm), and for oxalic acid 19.3 mM H_2SO_4 eluent ($\lambda_{detection}$ = 206 nm) were applied.

3. Results and discussion

3.1. Characterization of TiO_2-HSs

The CSs – which were used as templates for the shape-controlled synthesis – were characterized in detail in our previous publications [20,21,30]. For the purification of CSs various solvents (acetone or ethanol) were used, because – based on our previous results and the publication of Mahyar and Amani-Ghadim [34] – applying solvents of different polarity can result in the formation of titanium dioxides with different crystal phase compositions and characteristics. By the utilization of these CSs TiO_2-HSs were prepared (Table 1) applying different calcination temperatures (500, 800 °C), which were characterized by XRD, SEM and TEM in order to determine which TiO_2-HS possesses the best characteristics to be used as the base material for the deposition of noble metals.

The SEM and TEM micrographs of the TiO_2-HSs are shown in Fig. 1. Based on the SEM measurements it was found that the samples synthesized at similar conditions (Fig. 1a with Fig. 1b and Fig. 1c with Fig. 1d), *i.e.* same solvent and calcination temperature, similar characteristics could be observed (similar morphology and diameter/circularity values) (Table 1). Based on our previous work [20] the most

critical step during the synthesis of HSs *via* template removal is the elimination of CSs by calcination. In the case of samples calcined at 500 °C (Figs. 1a and b) well-defined spheres were observed possessing near perfect morphology, which were not damaged during calcination. The circularity values, medians and the diameter distribution histograms are summarized in Table 1 and Fig. S2, respectively. The TEM images of the samples calcined at 500 °C (Fig. 1e and f) confirmed that they had regular hollow cavities, as intended. The theoretical thickness of the TiO_2 shell – evaluated from the quantities of the reactants – was calculated to be 70 nm from the relative weight fractions of CS and TiO_2 coating (determined from the volume and density of these species). This value is in reasonably good accordance with the one obtained from the TEM micrographs, which was measured to be ~60 nm. By increasing the calcination temperature to 800 °C (Fig. 1c and d), it was found that hollow structures with raspberry-like surface were formed, in contrast with the smooth surfaces detected in the previous cases. It was also observed that the high temperature also caused the inner diameter of the hollow cavity to be smaller (Fig. 1g and h), which could be explained as the result of the sintering of the nanoparticles [35].

Subsequently, XRD and nitrogen adsorption measurements were carried out and the results (crystal phase composition, primary crystallite sizes, specific surface areas) are summarized in Table 1. As expected, the samples calcined at lower temperature (500 °C, $TiO_2\_HS_{500}^{Ac}$ and $TiO_2\_HS_{500}^{EtOH}$) mainly consisted of anatase, while samples calcined at the higher temperature (800 °C, $TiO_2\_HS_{800}^{Ac}$ and $TiO_2\_HS_{800}^{EtOH}$) contained predominantly rutile phase and larger crystallites. As for the N_2 adsorption measurements, despite having relatively low crystallite sizes (18–35 nm), the corresponding specific surface areas were surprisingly low (~6 $m^2 \cdot g^{-1}$ in all cases).

Summarizing these results, it was established, that sample $TiO_2\_HS_{500}^{Ac}$ possessed the best characteristics to be used as base material for the determination of photocatalytic activity gain caused by the unique morphology (highest circularity value, regular hollow cavity). Additionally, it was also the most appropriate from the economic point of view, since for the synthesis of this sample the CSs were purified by acetone, which is cheaper than ethanol, and for the elimination of the CSs only 500 °C temperature was applied making its production more cost-effective. Therefore, later on, for the deposition of noble metals this sample was selected as base material. Lastly, after the $TiO_2\_HS_{500}^{Ac}$ sample was chosen as base material, a reference sample was also synthesized in the same way just without the application of CS templates (denoted as '$TiO_2\_no\_HS_{500}^{Ac}$'), to investigate the possible effects of the hollow structure. This sample was also examined *via* SEM and TEM measurements (Fig. 2). Based on the SEM micrographs (Fig. 2a) it was observed that it also contained well-defined spheres with relatively high diameter (~1300 nm), comparable to prior samples. Then, this sample was investigated by TEM measurements as well (Fig. 2b) and it was found that it contained solely solid spheres, which, most importantly, makes it most suitable for the investigation of the effects caused by the hollow morphology in the case of our other samples. For the formation of spherical morphology (in the absence of CS templates in the case of sample $TiO_2\_no\_HS_{500}^{Ac}$), a plausible explanation can be that – according to the Ostwald ripening phenomenon – the formation of larger structures is thermodynamically favored as there are less molecules on the surface in an energetically less stable position, making the development of the spherical shape (with the smallest specific surface area) favored [36]. The reason for the relatively high diameter (low specific surface area) could be – as it was already observed in our previous work – that applying a precursor containing relatively long alkyl chains can result in slower hydrolysis making the formation of larger structures favored [37].

3.2. Further characterization of reference TiO_2-s and TiO_2-HSs modified with noble metals

Following the deposition of gold and platinum noble metals at

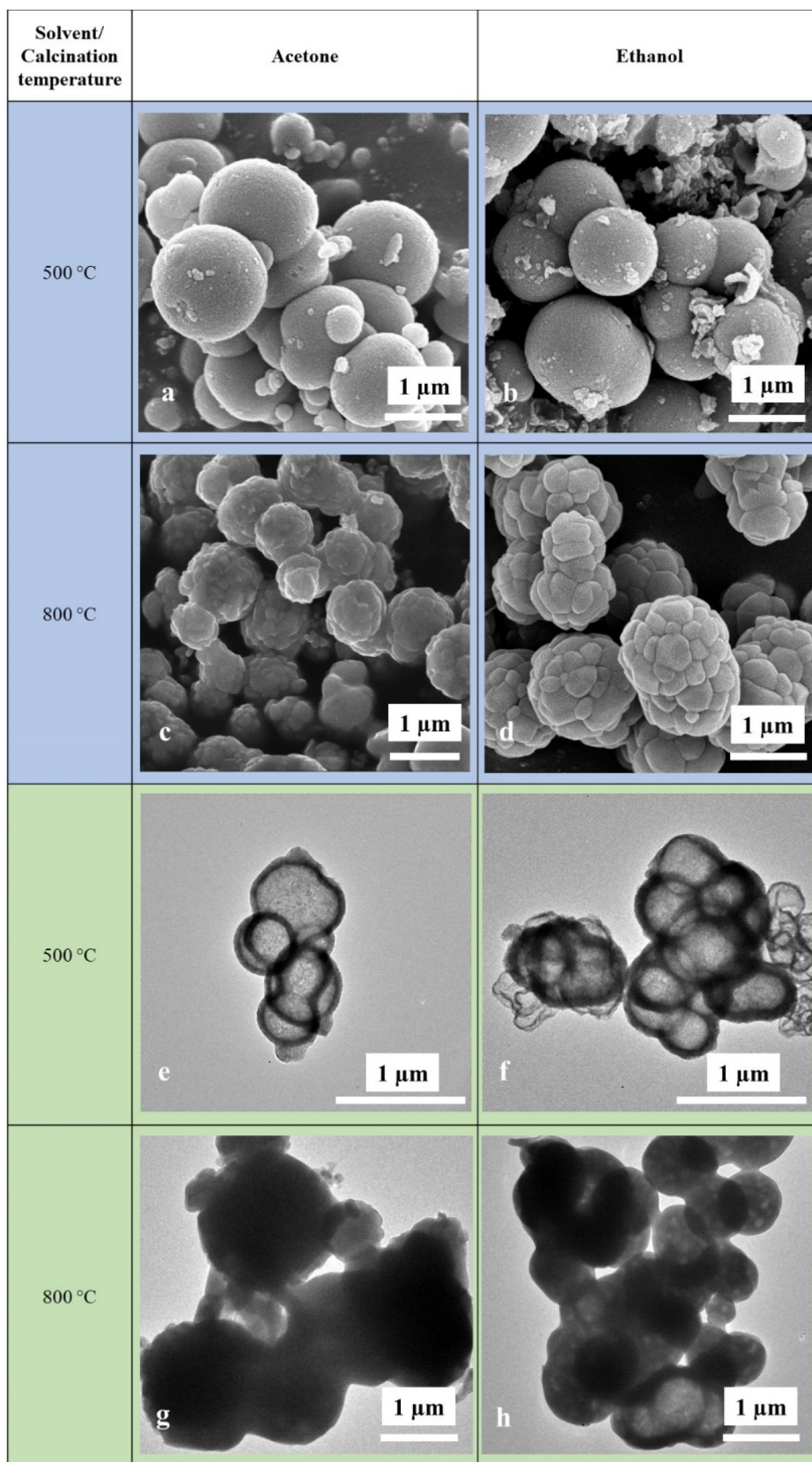**Fig. 1.** SEM micrographs of samples $TiO_2\_HS_{500}^{Ac}$ (a), $TiO_2\_HS_{500}^{EtOH}$ (b), $TiO_2\_HS_{800}^{Ac}$ (c) $TiO_2\_HS_{800}^{EtOH}$ (d) and their corresponding TEM figures (e-h, respectively).

0.25 wt% on the $TiO_2\_HS_{500}^{Ac}$ sample TEM images were recorded (Fig. 3a and c, respectively). It was observed, that even after the deposition process the regular hollow spherical morphology remained intact, the

noble metals were evenly distributed on the surface and no aggregation occurred. Additionally, HRTEM images were utilized to measure the d-spacing of the TiO_2 shell, the gold (Fig. 3b) and platinum (Fig. 3d)

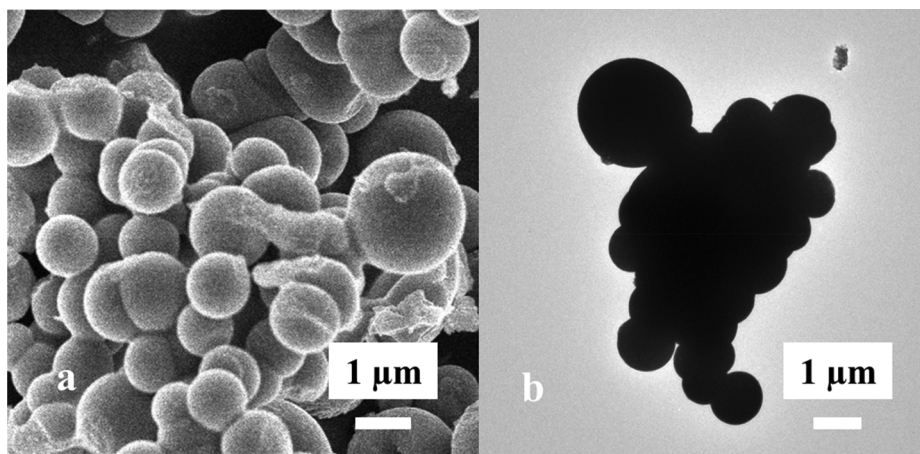**Fig. 2.** SEM (a) and TEM (b) images of reference non-hollow sample $TiO_2\_no\_HS_{500}^{Ac}$.

nanoparticles to confirm their presence. Accordingly, the measured 3.4 Å value was attributed to the TiO_2 (1 0 1) crystallographic plane, 2.4 Å to the Au (1 1 1) plane and 2.0 Å to the Pt (2 0 0) plane.

Then, XRD measurements were carried out to determine the influence of the chemical deposition process on the properties of the $TiO_2\_HS_{500}^{Ac}$ base material (Fig. S3, Table 1). It was found that after the deposition process the noble metal-containing samples largely retained their crystal phase composition as expected. The rutile crystal phase content of ~8–13 wt% of the base material and noble metal-containing samples could be beneficial in terms of the photocatalytic activity of

these samples similarly to the well-known commercial reference photocatalyst P25 [38]. The non-hollow $TiO_2\_no\_HS_{500}^{Ac}$ sample also contained rutile crystal phase in 3 wt%. Regarding the crystal phase compositions, it is well known that anatase – due to its large band gap (3.2 eV) – does not absorb visible light, whereas rutile has a narrower band gap (3.02 eV) making the absorption of visible light possible to a certain extent; a fact that can have a considerable influence on the resulting photocatalytic activities of the samples [39–41].

As the next step, the light absorption properties were investigated *via* DR measurements (Fig. 4). The band gap energies were determined
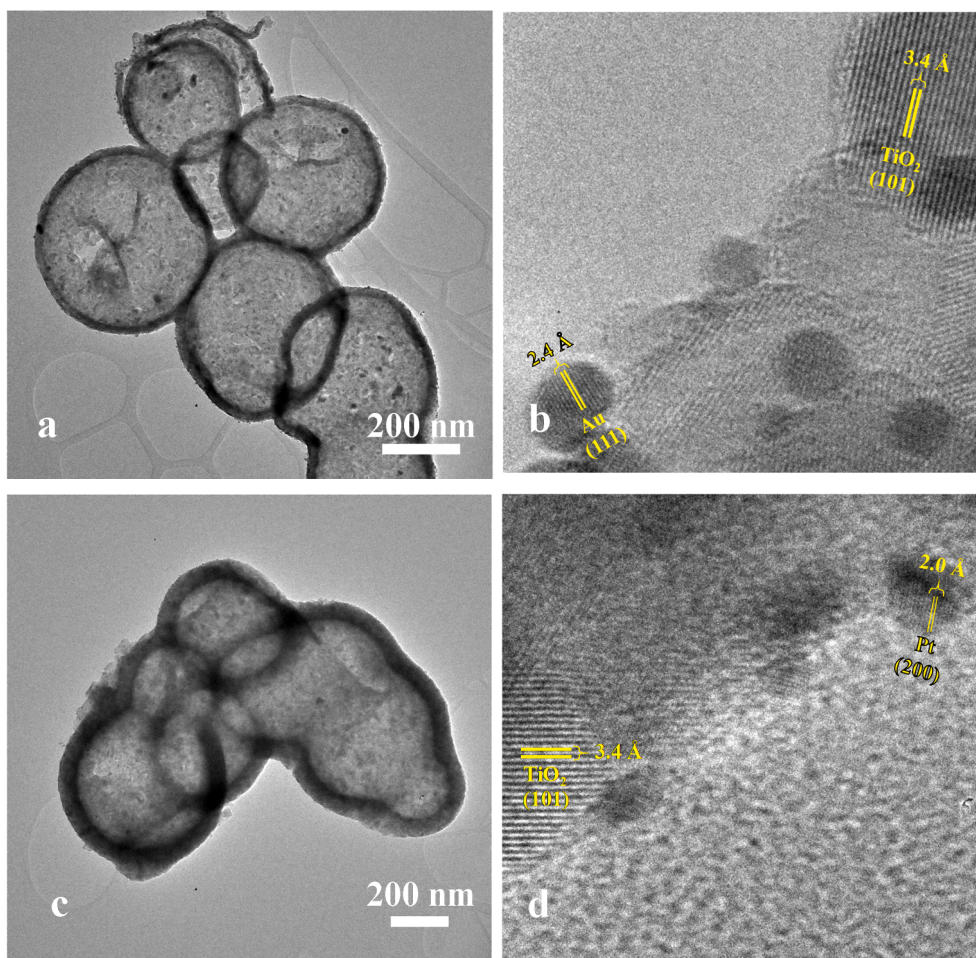

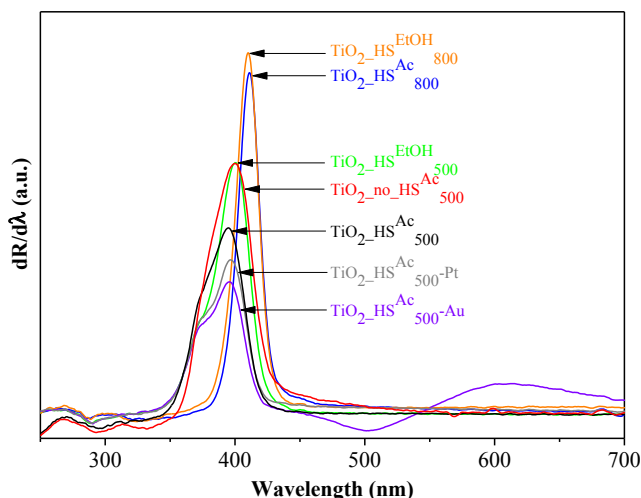**Fig. 3.** TEM images of samples $TiO_2\_HS_{500}^{Ac}$-Au (a, b) and $TiO_2\_HS_{500}^{Ac}$-Pt (c, d).

Fig. 4. First order derivative DR spectra of the as-prepared photocatalysts.

from the first order derivatives of the DR spectra of the TiO_2–s, because based on the publication of Flak et al. the excitability of the photocatalysts can be determined more reliably by plotting the first-order derivatives of the DR spectra as a function of wavelength [42]. As expected, rutile phase TiO_2-s possessed lower band gaps (3.02 eV for $TiO_2\_HS_{800}^{Ac}$ and $TiO_2\_HS_{800}^{EtOH}$) compared to the anatase phase TiO_2-s (3.1 eV for $TiO_2\_no\_HS_{500}^{Ac}$, $TiO_2\_HS_{500}^{EtOH}$ and 3.14 eV for $TiO_2\_HS_{500}^{Ac}$). The band gap after noble metal deposition (3.13 eV for both $TiO_2\_HS_{500}^{Ac}$-Au and $TiO_2\_HS_{500}^{Ac}$-Pt) did not change significantly compared to the base material ($TiO_2\_HS_{500}^{Ac}$, 3.14 eV). The inflection point at ~542 nm in the derivative spectrum can be attributed to the plasmon resonance of the gold nanoparticles in the case of sample TiO_2-HS_{500}^{Ac}-Au.

The surface properties were examined by FT-IR measurements (Fig. 5). The bands at 424, 515 and 620 cm^{-1} can be attributed to the transverse optical vibrations of the Ti–O bonds [43–45]. The shape of these bands varied in accordance with the different crystal phases; anatase has less defined Ti–O stretch band as it possesses less ordered structure (compared to rutile), consequently, in the case of mixed crystal phase compositions, the infrared absorption bands also represented this transmission between the two crystal phases [46]. The doublet at 2340, 2358 cm^{-1} is characteristic of adsorbed CO_2 [47]. Additional bands which could be ascribed to leftover carbon from either the TiO_2 precursor or the CS templates were not observed, from which
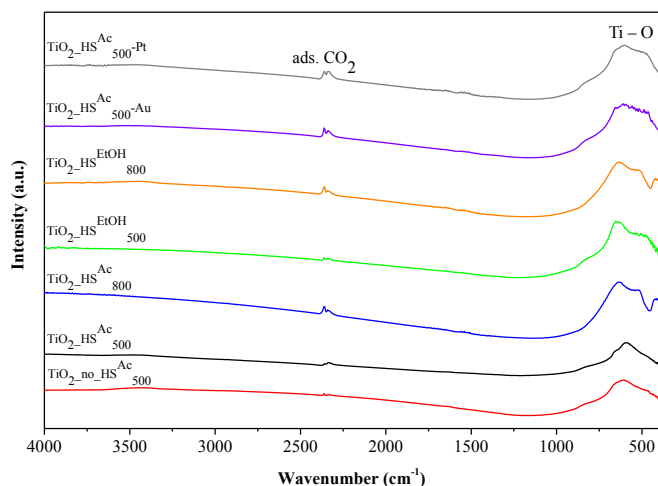
it was concluded that during the calcination process these were entirely eliminated from the system.

3.3. Evaluation of photocatalytic activity

The photocatalytic activities of the non-hollow, spherical reference sample ($TiO_2\_no\_HS_{500}^{Ac}$), the base material ($TiO_2\_HS_{500}^{Ac}$) and the noble metal-containing samples ($TiO_2\_HS_{500}^{Ac}$-Au and $TiO_2\_HS_{500}^{Ac}$-Pt) were investigated by the photocatalytic degradation of phenol and oxalic acid under UV and visible light irradiation and the results were summarized in Fig. 6 (UV irradiation) and Fig. S4 (visible light irradiation). Additionally, the photocatalytic activities of solid spherical $TiO_2\_no\_HS_{500}^{Ac}$-Au and $TiO_2\_no\_HS_{500}^{Ac}$-Pt samples were also investigated in the case of phenol degradation under UV light irradiation.

In the case of the spherical, but non-hollow $TiO_2\_no\_HS_{500}^{Ac}$ reference sample negligible photocatalytic activity was observed under visible light irradiation (~3–4% model pollutants were degraded) and by applying UV irradiation 26% phenol and 36% oxalic acid were degraded after the 240-minute-long measurements.

As the next step, the hollow spherical base material ($TiO_2\_HS_{500}^{Ac}$) was investigated, to determine the possible achievable effects of the unique morphology on the photocatalytic activity. In almost every case, the enhancement of photocatalytic activity was observed (except in the case of oxalic acid degradation under visible light irradiation). In the case of visible light irradiation only negligible differences were observed, however, under UV light irradiation notable 166% and 135% enhancements were detected for phenol and oxalic acid degradations, respectively, compared to the non-hollow reference TiO_2.

By the deposition of noble metals on the surface of the hollow spherical base catalyst $TiO_2\_HS_{500}^{Ac}$, in almost every case the photocatalytic activity increased (except in the case of $TiO_2\_HS_{500}^{Ac}$-Au during the decomposition of phenol under UV light irradiation). Applying visible light irradiation 156% and 66% increases were observed in the degradation rate of phenol for sample TiO_2-HS_{500}^{Ac}_Au and $TiO_2\_HS_{500}^{Ac}$-Pt, respectively, which values were 780% and 200% for oxalic acid, respectively. At the same time, in the case of UV irradiation these values were −20%, 30% and 18%, 18%, respectively.

Then, after comparing the photocatalytic activity difference between (i) the bare solid spherical ($TiO_2\_no\_HS_{500}^{Ac}$) and bare hollow spherical ($TiO_2\_HS_{500}^{Ac}$) samples (3rd paragraph), (ii) the bare hollow spherical ($TiO_2\_HS_{500}^{Ac}$) and noble metal-containing hollow spherical ($TiO_2\_HS_{500}^{Ac}$_Au and $TiO_2\_HS_{500}^{Ac}$-Pt) samples (4th paragraph), finally, the photocatalytic activity difference between (iii) the noble metal-containing solid spherical ($TiO_2\_no\_HS_{500}^{Ac}$_Au and $TiO_2\_no\_HS_{500}^{Ac}$-Pt) and noble metal-containing hollow spherical samples ($TiO_2\_HS_{500}^{Ac}$_Au and $TiO_2\_HS_{500}^{Ac}$-Pt) were investigated additionally, for phenol degradation under UV light irradiation (Fig. 6 left side). It was found that the photocatalytic activities of hollow spherical samples were always higher compared to the solid spherical samples, further reinforcing the beneficial effect of the unique hollow spherical morphology on the photocatalytic performance. The $TiO_2\_HS_{500}^{Ac}$_Au sample was more efficient by 81% compared to $TiO_2\_no\_HS_{500}^{Ac}$_Au, while $TiO_2\_HS_{500}^{Ac}$_Pt was more efficient by 18% compared to $TiO_2\_no\_HS_{500}^{Ac}$_Pt in terms of total degraded phenol amount.

For the explanation of the obtained results, numerous factors can be considered: (i) properties of the TiO_2 (crystallite size, specific surface area, crystal phase composition, surface features, etc.) [16,48–50]; (ii) properties of the noble metal (size, shape, number) [14,15,51,52]; (iii) properties of the model pollutants (adsorption ability, charge carrier-scavenging attributes, features of intermediates, etc.) [14–16,48]; (iv) the emission spectrum of the light source and the temperature during the photocatalytic experiments [53–55].

Generally, it can be said that the investigated titania decomposed oxalic acid to a greater degree compared to phenol. It is well-known, that phenol is a poorly adsorbing compound and the degradation of pollutants takes place by the utilization of the generated ·OH radicals

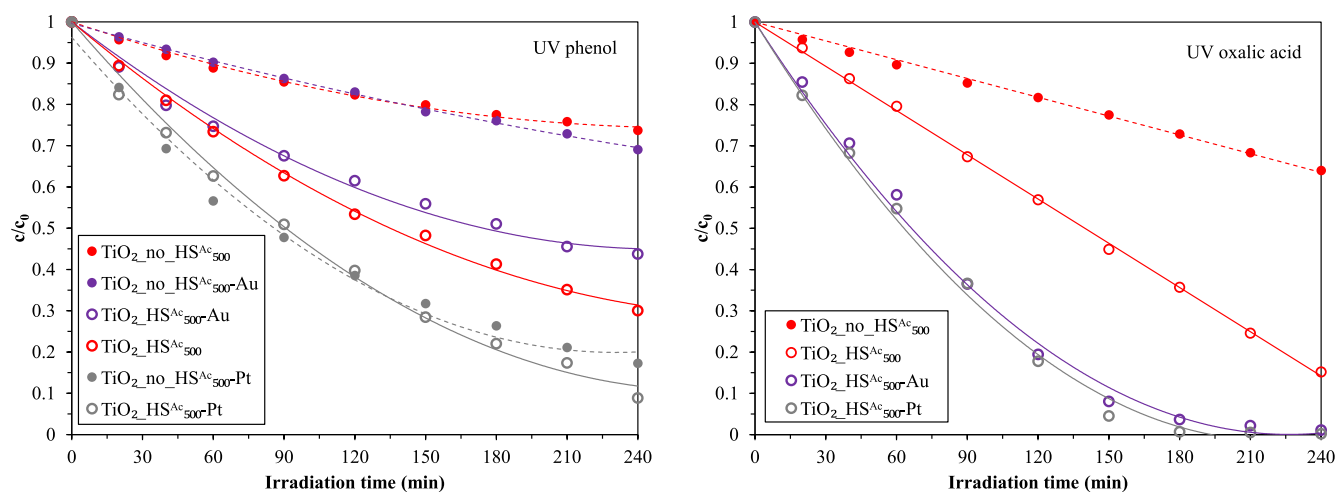**Fig. 5.** FT-IR spectra of the investigated photocatalysts.

Fig. 6. Photocatalytic activity of the investigated photocatalysts under UV light irradiation.

[56]; moreover, the forming degradation intermediates with different adsorption properties can also block the active sites of the photocatalyst hindering the further degradation process. Conversely, oxalic acid can adsorb to the surface of TiO_2 extremely well facilitating its degradation by the generated charge carriers; furthermore, oxalic acid is a hole scavenger resulting in the efficient separation/increased lifespan of the electron-hole pairs [15].

In the case of oxalic acid degradation, the addition of Pt and Au nanoparticles resulted in the increase of photocatalytic activity in all cases (under both UV and visible light irradiation), reaching nearly 100% degradation efficiency in the former case. This result is in good accordance with literature data where the same results were observed in the case of commercial (predominantly) anatase phase TiO_2-s (Aldrich anatase, Aeroxide P25) [15,16]. The photocatalytic activity enhancement of TiO_2-HS_{500}^{Ac}-Pt can be explained by a double charge trapping mechanism: oxalic acid acts as a hole scavenger, whereas the Pt separates the electron from the TiO_2 nanoparticle [14]. In the case of $TiO_2\_HS_{500}^{Ac}$-Au the photocatalytic activity enhancement can be associated with the results of our previous work, where the highest degree of photocatalytic activity gain was observed in the presence of spherical gold nanoparticles [52], similar to our present results (Fig. 3b).

As for the phenol degradation tests, only in the case of $TiO_2\_HS_{500}^{Ac}$-Au sample under UV light irradiation was a photocatalytic activity decrease observed, which is in good accordance with the literature data: it is well-known, that in the case of commercial Aeroxide P25 (which has similar crystal phase composition compared to our samples) the deposition of gold nanoparticles results in decreased photocatalytic activity in the case of phenol under UV light irradiation [16,51,52,57]. However, in the case of the gold-deposited sample under visible light irradiation a photocatalytic activity enhancement was observed, which can be explained by the fact, that the electrons formed by surface plasmon resonance excitation can be efficiently injected into the conduction band of TiO_2 leading to enhanced charge separation [58]. The fact, that the surface resonance peak of gold is located in the visible light range, could explain the observed photocatalytic activity enhancement under visible light irradiation. In the case of $TiO_2\_HS_{500}^{Ac}$-Pt sample the photocatalytic activity increased after the deposition of platinum under both visible and UV light irradiation. The photocatalytic activity gain – in the case of visible light irradiation – could be attributed to the rutile content of the sample, since electron trapping by platinum is much more significant on rutile than on anatase [59]. However, the photocatalytic activity enhancement observed in the case of our $TiO_2\_HS_{500}^{Ac}$-Pt sample under UV irradiation could not be attributed to literature data, as normally the deposition of platinum nanoparticles on Aeroxide P25 (possessing similar crystal phase composition) leads to decreased photocatalytic activity [15,60]. For the deeper

understanding of the as-mentioned results in the next paragraph the unique hollow spherical morphology of our samples was taken into account.

It is well-known that light waves (used for the excitation of the photocatalysts) cannot only interact with matter but with each other as well, which is called wave interference. Constructive interference occurs, if the crests of one wave overlap the crests of the other wave. For this to happen, the distance between two waves must be equal to an integer multiple of the wavelength and as a result, the crests combine to produce a wave with greater amplitude. If we excite our photocatalyst with such light waves with greater amplitude, then the excitation process can be more efficient resulting in higher photocatalytic activity. Based on this theory, the following steps were taken: the emission spectra of the applied lamps (Fig. S1) were compared to the diameter distribution histograms (Fig. S2) and it was ascertained, that what proportion of the hollow spheres happens to be precisely in the range where the travelled distance is the integer multiple of the wavelength of the emission maxima. For the calculations the most intense domain of the emission spectrum (360 ± 10 nm) was taken into account. Then, the percentage of the hollow spheres with valid resonance condition – where the constructive interference of the light waves can most probably occur – was counted, by dividing the diameter of the hollow spheres by the wavelength of the light source. After these calculations were carried out, the as-calculated data were compared to the photocatalytic activities (Fig. 6 left side) and these results are represented in Fig. 7. It can be seen in the figure, that the observed photocatalytic activity ($TiO_2\_HS_{500}^{Ac}$-Au < $TiO_2\_HS_{500}^{Ac}$ < $TiO_2\_HS_{500}^{Ac}$-Pt) indeed corresponds well to the increasing ratio of hollow spheres with valid resonance condition. Since it is well-known, that the excitability of a photocatalyst correlates with the intensity of the light source, and that the intensity of a wave is proportional to the square of its amplitude, then it can be expected, that after constructive interference occurs resulting in the increase of the amplitude, the light waves with higher intensity could indeed cause the enhancement of the photocatalytic activity. The validity of this phenomenon was further reinforced by the results mentioned in the 5th paragraph: if we compare the 3 hollow spherical samples appearing in Fig. 7 with their solid spherical counterparts, it is apparent that the hollow spherical samples were indeed more efficient in the degradation of phenol under UV light irradiation.

To sum up, based on the results of the photocatalytic activity experiments, it was observed that in each case reference solid spherical TiO_2 samples proved to be less efficient compared to their hollow spherical counterparts. The unique morphology indeed increased the photocatalytic activity, as did the deposition of noble metals in most cases, thus the combination of the two photocatalytic activity enhancing methods was successful.
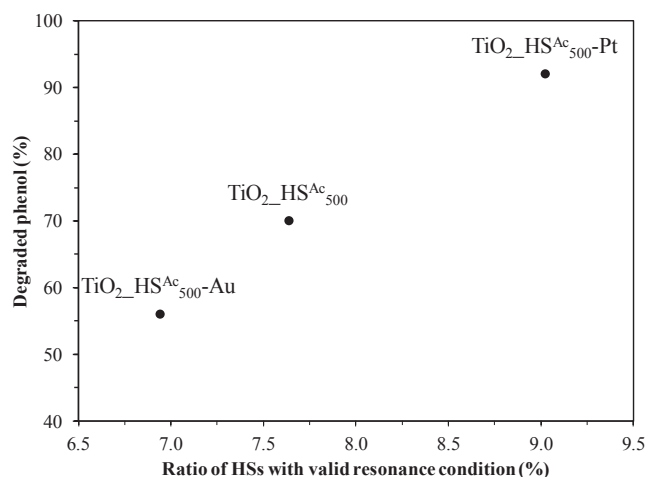
Fig. 7. Comparison of the ratio of TiO$_2$-HSs with enhanced light trapping properties to the observed amount of degraded phenol model pollutant under UV light irradiation by the end of the 240-min-long experiments.

4. Conclusions

Carbon spheres were used as templates to synthesize titanium dioxide hollow spheres applying different synthesis parameters (CS purification solvent, calcination temperature). The CS purification solvent (acetone or ethanol) did not influence the characteristics of the TiO$_2$-HSs, whereas applying 500 °C calcination temperature resulted in anatase phase TiO$_2$-HSs with perfect hollow spherical morphology, while applying 800 °C yielded rutile phase TiO$_2$-HSs with less regular morphology.

The TiO$_2$-HS possessing the best properties in terms of morphology was selected for the deposition of gold and platinum nanoparticles in 0.25 wt%. SEM and TEM measurements confirmed, that the morphology remained intact after the deposition process and that the noble metal nanoparticles were distributed evenly on the TiO$_2$-HSs.

The photocatalytic activity enhancement caused by either the unique morphology and the presence of noble metals was investigated by the degradation of phenol and oxalic acid under both UV and visible light irradiation using the base hollow spherical, and solid (non-hollow) spherical TiO$_2$-s as references. The hollow spherical morphology resulted in remarkable 166% and 135% increases in photocatalytic activity during UV light irradiation compared to the non-hollow solid reference sample in the case of phenol and oxalic acid, respectively. Using the same reference, after combining the hollow spherical morphology with the deposition of noble metals in the case of the gold-deposited sample these values were 113% and 178% for phenol, along with 246% and 178% for oxalic acid in the case of platinum-deposited TiO$_2$-s, respectively, under UV light irradiation. Summarizing, in the case of visible light irradiation, the gold-deposited hollow spherical TiO$_2$ had the best photocatalytic activity, while in the case of UV irradiation the platinum containing hollow spherical TiO$_2$ proved to be the most efficient for the degradation of both oxalic acid and phenol.

Unusual photocatalytic activity order was observed in the case of UV irradiation during the decomposition of phenol, and for its elucidation the solid spherical counterparts of each hollow spherical sample were applied to propose a plausible explanation. It was presumed that the hollow spherical TiO$_2$-s have increased light harvesting properties, and the ratio of hollow spheres with this unique feature was calculated. The photocatalytic activity indeed increased with increasing proportions of titanium dioxide hollow sphere diameters close to the integer multiple of the excitation light source's wavelength, *i.e.* in which case the occurrence of constructive interference was more probable. The proposed explanation was in good agreement with the acquired results,

since the hollow spherical TiO$_2$-s were always more efficient compared to their solid spherical counterparts.

CRediT authorship contribution statement

Tamás Gyulavári: Investigation, Writing - original draft, Conceptualization. **Kata Kovács:** Investigation. **Zoltán Kovács:** Conceptualization. **Enikő Bárdos:** Investigation. **Gábor Kovács:** Writing - review & editing. **Kornélia Baán:** Investigation. **Klára Magyari:** Investigation. **Gábor Veréb:** Writing - review & editing. **Zsolt Pap:** Supervision, Writing - original draft. **Klara Hernadi:** Funding acquisition, Writing - review & editing. **:** .

Declaration of Competing Interest

The authors declare that they have no known competing financial interests or personal relationships that could have appeared to influence the work reported in this paper.

Appendix A. Supplementary data

Supplementary data to this article can be found online at https://doi.org/10.1016/j.apsusc.2020.147327.

References

[1] Y. Lu, L. Hao, K. Matsuzaka, H. Yoshida, H. Asanuma, J. Chen, F. Pan, Titanium dioxide–nickel oxide composite coatings: preparation by mechanical coating/thermal oxidation and photocatalytic activity, Mater. Sci. Semicond. Process. 24 (2014) 138–145.
[2] É. Karácsonyi, L. Baia, A. Dombi, V. Danciu, K. Mogyorósi, L.C. Pop, G. Kovács, V. Coşoveanu, A. Vulpoi, S. Simon, Z. Pap, The photocatalytic activity of TiO$_2$/WO$_3$/noble metal (Au or Pt) nanoarchitectures obtained by selective photodeposition, Catal. Today 208 (2013) 19–27.
[3] R.K. Mandal, S. Kundu, S. Sain, S.K. Pradhan, Enhanced photocatalytic performance of V2O5–TiO2 nanocomposites synthesized by mechanical alloying with morphological hierarchy, New J. Chem. 43 (2019) 2804–2816.
[4] N.O. Balayeva, M. Fleisch, D.W. Bahnemann, Surface-grafted WO$_3$/TiO$_2$ photocatalysts: Enhanced visible-light activity towards indoor air purification, Catal. Today 313 (2018) 63–71.
[5] C. Pablos, J. Marugan, R. van Grieken, P.S.M. Dunlop, J.W.J. Hamilton, D.D. Dionysiou, J.A. Byrne, Electrochemical enhancement of photocatalytic disinfection on aligned TiO$_2$ and nitrogen doped TiO(2) nanotubes, Molecules 22 (2017).
[6] A. Gil, A.M. García, M. Fernández, M.A. Vicente, B. González-Rodríguez, V. Rives, S.A. Korili, Effect of dopants on the structure of titanium oxide used as a photocatalyst for the removal of emergent contaminants, J. Ind. Eng. Chem. 53 (2017) 183–191.
[7] A. Samokhvalov, Hydrogen by photocatalysis with nitrogen codoped titanium dioxide, Renew. Sust. Energ. Rev. 72 (2017) 981–1000.
[8] M.C. Wu, J. Hiltunen, A. Sapi, A. Avila, W. Larsson, H.C. Liao, M. Huuhtanen, G. Toth, A. Shchukarev, N. Laufer, A. Kukovecz, Z. Konya, J.P. Mikkola, R. Keiski, W.F. Su, Y.F. Chen, H. Jantunen, P.M. Ajayan, R. Vajtai, K. Kordas, Nitrogen-doped anatase nanofibers decorated with noble metal nanoparticles for photocatalytic production of hydrogen, ACS Nano 5 (2011) 5025–5030.
[9] R. Kun, S. Tarján, A. Oszkó, T. Seemann, V. Zöllmer, M. Busse, I. Dékány, Preparation and characterization of mesoporous N-doped and sulfuric acid treated anatase TiO$_2$ catalysts and their photocatalytic activity under UV and Vis illumination, J. Solid State Chem. 182 (2009) 3076–3084.
[10] M. Gratzel, Solar energy conversion by dye-sensitized photovoltaic cells, Inorg. Chem. 44 (2005) 6841–6851.
[11] Z. Youssef, L. Colombeau, N. Yesmurzayeva, F. Baros, R. Vanderesse, T. Hamieh, J. Toufaily, C. Frochot, T. Roques-Carmes, S. Acherar, Dye-sensitized nanoparticles for heterogeneous photocatalysis: Cases studies with TiO$_2$, ZnO, fullerene and

graphene for water purification, Dyes Pigm. 159 (2018) 49–71.

[12] Á. Kmetykó, Á. Szániel, C. Tsakiroglou, A. Dombi, K. Hernádi, Enhanced photo-catalytic H₂ generation on noble metal modified TiO2 catalysts excited with visible light irradiation, React. Kinet. Mech. Catal. 117 (2015) 379–390.

[13] Z. Wei, M. Janczarek, M. Endo, K. Wang, A. Balčytis, A. Nitta, M.G. Méndez-Medrano, C. Colbeau-Justin, S. Juodkazis, B. Ohtani, E. Kowalska, Noble metal-modified faceted anatase titania photocatalysts: octahedron versus decahedron, Appl. Catal. B Environ. 237 (2018) 574–587.

[14] S. Fodor, G. Kovács, K. Hernádi, V. Danciu, L. Baia, Z. Pap, Shape tailored Pd na-noparticles' effect on the photocatalytic activity of commercial TiO₂, Catal. Today 284 (2017) 137–145.

[15] G. Kovács, S. Fodor, A. Vulpoi, K. Schrantz, A. Dombi, K. Hernádi, V. Danciu, Z. Pap, L. Baia, Polyhedral Pt vs. spherical Pt nanoparticles on commercial titanias: Is shape tailoring a guarantee of achieving high activity? J. Catal. 325 (2015) 156–167.

[16] Z.-R. Tóth, G. Kovács, K. Hernádi, L. Baia, Z. Pap, The investigation of the photo-catalytic efficiency of spherical gold nanocages/TiO₂ and silver nanospheres/TiO₂ composites, Sep. Purif. Technol. 183 (2017) 216–225.

[17] C.-C. Nguyen, N.-N. Vu, T.-O. Do, Efficient hollow double-shell photocatalysts for the degradation of organic pollutants under visible light and in darkness, J. Mater. Chem. A 4 (2016) 4413–4419.

[18] Y. Zou, J.-W. Shi, D. Ma, Z. Fan, L. Lu, C. Niu, In situ synthesis of C-doped TiO₂@g-C 3 N 4 core-shell hollow nanospheres with enhanced visible-light photocatalytic activity for H 2 evolution, Chem. Eng. J. 322 (2017) 435–444.

[19] L. Xiang, X. Zhao, Wet-Chemical Preparation of TiO₂-Based Composites with Different Morphologies and Photocatalytic Properties, Nanomater. 7 (2017).

[20] T. Gyulavari, G. Vereb, Z. Pap, B. Reti, K. Baan, M. Todea, K. Magyari, I.M. Szilagyi, K. Hernadi, Utilization of carbon nanospheres in photocatalyst production: from composites to highly active hollow structures, Materials 12 (2019).

[21] N. Justh, L.P. Bakos, K. Hernadi, G. Kiss, B. Reti, Z. Erdelyi, B. Parditka, I.M. Szilagyi, Photocatalytic hollow TiO₂ and ZnO nanospheres prepared by atomic layer deposition, Sci. Rep. 7 (2017) 4337.

[22] W. Raza, M.M. Haque, M. Muneer, D. Bahnemann, Synthesis of visible light driven TiO2 coated carbon nanospheres for degradation of dyes, Arab. J. Chem. (2015).

[23] Y. Ao, J. Xu, D. Fu, C. Yuan, A simple method for the preparation of titania hollow sphere, Catal. Commun. 9 (2008) 2574–2577.

[24] K. Lv, J. Li, X. Qing, W. Li, Q. Chen, Synthesis and photo-degradation application of WO3/TiO2 hollow spheres, J. Hazard. Mater. 189 (2011) 329–335.

[25] S. Semlali, T. Pigot, D. Flahaut, J. Allouche, S. Lacombe, L. Nicole, Mesoporous Pt-TiO2 thin films: photocatalytic efficiency under UV and visible light, Appl. Catal. B Environ. 150–151 (2014) 656–662.

[26] K. Mogyorósi, Á. Kmetykó, N. Czirbus, G. Veréb, P. Sipos, A. Dombi, Comparison of the substrate dependent performance of Pt-, Au- and Ag-doped TiO₂ photocatalysts in H2-production and in decomposition of various organics, React. Kinet. Catal. Lett. 98 (2009) 215–225.

[27] G.N. Nomikos, P. Panagiotopoulou, D.I. Kondarides, X.E. Verykios, Kinetic and mechanistic study of the photocatalytic reforming of methanol over Pt/TiO₂ cata-lyst, Appl. Catal. B Environ. 146 (2014) 249–257.

[28] L. Liu, J. Yang, S. Liu, L. Bai, B. Liu, Q. Wang, G. Xu, P. Jing, S. Yu, J. Zhang, Hollow hybrid titanate/Au@TiO₂ hierarchical architecture for highly efficient photo-catalytic application, Catal. Commun. 54 (2014) 66–71.

[29] E. Grabowska, M. Marchelek, T. Klimczuk, G. Trykowski, A. Zaleska-Medynska, Noble metal modified TiO₂ microspheres: surface properties and photocatalytic activity under UV–vis and visible light, J. Mol. Catal. A: Chem. 423 (2016) 191–206.

[30] B. Réti, G.I. Kiss, T. Gyulavári, K. Baan, K. Magyari, K. Hernadi, Carbon sphere templates for TiO₂ hollow structures: preparation, characterization and photo-catalytic activity, Catal. Today 284 (2017) 160–168.

[31] R.A. Spurr, H. Myers, Quantitative analysis of anatase-rutile mixtures with an X-ray diffractometer, Anal. Chem. 29 (1957) 760–762.

[32] H. Zhang, J.F. Banfield, Understanding polymorphic phase transformation behavior during growth of nanocrystalline aggregates: insights from TiO₂, J. Phys. Chem. B 104 (2000) 3481–3487.

[33] E.P. Cox, A method of assigning numerical and percentage values to the degree of roundness of sand grains, J. Paleontol. 1 (1927) 179–183.

[34] A. Mahyar, A.R. Amani-Ghadim, Influence of solvent type on the characteristics and photocatalytic activity of TiO₂ nanoparticles prepared by the sol–gel method, Micro Nano Lett. 6 (2011) 244.

[35] S.J. Kalita, S. Qiu, S. Verma, A quantitative study of the calcination and sintering of nanocrystalline titanium dioxide and its flexural strength properties, Mater. Chem. Phys. 109 (2008) 392–398.

[36] P. Wang, L. Yang, L. Wang, J. Zhang, Template-free synthesis of hollow anatase TiO₂ microspheres through stepwise water-releasing strategy, Mater. Lett. 164 (2016) 405–408.

[37] P. Berki, B. Reti, K. Terzi, I. Bountas, E. Horvath, D. Fejes, A. Magrez, C. Tsakiroglu, L. Forró, K. Hernadi, The effect of titania precursor on the morphology of prepared TiO₂/MWCNT nanocomposite materials, Phys. Status Solidi B 251 (2014)

2384–2388.

[38] K.E. Rajashekhar, L.G. Devi, Polymorphic phase transformation of Degussa P25 TiO₂ by the chelation of diaminopyridine on TiO₆²⁻ octahedron: Correlation of anatase to rutile phase ratio on the photocatalytic activity, J. Mol. Catal. A: Chem. 374–375 (2013) 12–21.

[39] S. Yin, H. Hasegawa, D. Maeda, M. Ishitsuka, T. Sato, Synthesis of visible-light-active nanosize rutile titania photocatalyst by low temperature dis-solution–reprecipitation process, J. Photochem. Photobiol. A Chem. 163 (2004) 1–8.

[40] J. Noh, M. Yi, S. Hwang, K.M. Im, T. Yu, J. Kim, A facile synthesis of rutile-rich titanium oxide nanoparticles using reverse micelle method and their photocatalytic applications, J. Ind. Eng. Chem. 33 (2016) 369–373.

[41] S. Banerjee, J. Gopal, P. Muraleedharan, A.K. Tyagi, B. Rai, Physics and chemistry of photocatalytic titanium dioxide: Visualization of bactericidal activity using atomic force microscopy, Curr. Sci. 90 (2006) 1378–1383.

[42] D. Flak, A. Braun, B.S. Mun, J.B. Park, M. Parlinska-Wojtan, T. Graule, M. Rekas, Spectroscopic assessment of the role of hydrogen in surface defects, in the electronic structure and transport properties of TiO₂, ZnO and SnO₂ nanoparticles, Phys. Chem. Chem. Phys. 15 (2013) 1417–1430.

[43] T. Busani, R.A.B. Devine, Dielectric and infrared properties of TiO₂ films containing anatase and rutile, Semicond. Sci. Technol. 20 (2005) 870–875.

[44] M.R. Ayers, A.J. Hunt, Titanium oxide aerogels prepared from titanium metal and hydrogen peroxide, Mater. Lett. 34 (1998) 290–293.

[45] V. Maria Vinosel, M. Asisi Janifer, S. Anand, S. Pauline, Structural and functional group characterization of nanocomposite Fe₃O₄/TiO₂ and Its magnetic property, Mech. Mater. Sci. Eng. (2017).

[46] N.T. Nolan, M.K. Seery, S.C. Pillai, Spectroscopic investigation of the anatase-to-rutile transformation of Sol−Gel-Synthesized TiO₂ photocatalysts, J. Phys. Chem. C 113 (2009) 16151–16157.

[47] J. Orlikowski, B. Tryba, J. Ziebro, A.W. Morawski, J. Przepiórski, A new method for preparation of rutile phase titania photoactive under visible light, Catal. Commun. 24 (2012) 5–10.

[48] L. Baia, A. Vulpoi, T. Radu, É. Karácsonyi, A. Dombi, K. Hernádi, V. Danciu, S. Simon, K. Norén, S.E. Canton, G. Kovács, Z. Pap, TiO₂/WO₃/Au nanoarchi-tectures' photocatalytic activity "from degradation intermediates to catalysts' structural peculiarities" Part II: Aerogel based composites – fine details by spec-troscopic means, Appl. Catal. B Environ. 148–149 (2014) 589–600.

[49] H.P. Boehm, Acidic and basic properties of hydroxylated metal oxide surfaces, Discuss. Faraday Soc. 52 (1971) 264.

[50] M.A. Fox, M.T. Dulay, Heterogeneous photocatalysis, Chem. Rev. 93 (1993) 341–357.

[51] G. Kovács, L. Baia, A. Vulpoi, T. Radu, É. Karácsonyi, A. Dombi, K. Hernádi, V. Danciu, S. Simon, Z. Pap, TiO₂/WO₃/Au nanoarchitectures' photocatalytic ac-tivity, "from degradation intermediates to catalysts' structural peculiarities", Part I: Aeroxide P25 based composites, Appl. Catal. B Environ. 147 (2014) 508–517.

[52] Z. Pap, Z.R. Toth, V. Danciu, L. Baia, G. Kovacs, Differently Shaped Au Nanoparticles: A Case Study on the Enhancement of the Photocatalytic Activity of Commercial TiO₂, Materials 8 (2014) 162–180.

[53] Q. Hu, B. Liu, Z. Zhang, M. Song, X. Zhao, Temperature effect on the photocatalytic degradation of methyl orange under UV-vis light irradiation, Journal of Wuhan University of Technology-Mater. Sci. Ed., 25 (2010) 210-213.

[54] K. Nishijima, B. Ohtani, X. Yan, T.-A. Kamai, T. Chiyoya, T. Tsubota, N. Murakami, T. Ohno, Incident light dependence for photocatalytic degradation of acetaldehyde and acetic acid on S-doped and N-doped TiO2 photocatalysts, Chem. Phys. 339 (2007) 64–72.

[55] C.u. Gomes Silva, R. Juárez, T. Marino, R. Molinari, H. García, Influence of Excitation Wavelength (UV or Visible Light) on the Photocatalytic Activity of Titania Containing Gold Nanoparticles for the Generation of Hydrogen or Oxygen from Water, J. Am. Chem. Soc., 133 (2011) 595-602.

[56] G. Veréb, L. Manczinger, G. Bozsó, A. Sienkiewicz, L. Forró, K. Mogyorósi, K. Hernádi, A. Dombi, Comparison of the photocatalytic efficiencies of bare and doped rutile and anatase TiO₂ photocatalysts under visible light for phenol de-gradation and E. coli inactivation, Appl. Catal. B Environ. 129 (2013) 566–574.

[57] G. Veréb, Z. Ambrus, Z. Pap, Á. Kmetykó, A. Dombi, V. Danciu, A. Cheesman, K. Mogyorósi, Comparative study on UV and visible light sensitive bare and doped titanium dioxide photocatalysts for the decomposition of environmental pollutants in water, Appl. Catal. A Gen. 417–418 (2012) 26–36.

[58] Z. Xu, M. Quintanilla, F. Vetrone, A.O. Govorov, M. Chaker, D. Ma, Harvesting lost photons: plasmon and upconversion enhanced broadband photocatalytic activity in Core@Shell microspheres based on lanthanide-doped NaYF₄, TiO₂, and Au, Adv. Funct. Mater. 25 (2015) 2950–2960.

[59] T.A. Egerton, J.A. Mattinson, The influence of platinum on UV and 'visible' pho-tocatalysis by rutile and Degussa P25, J. Photochem. Photobiol. A Chem. 194 (2008) 283–289.

[60] B. Sun, A.V. Vorontsov, P.G. Smirniotis, Role of platinum deposited on TiO₂ in phenol photocatalytic oxidation, Langmuir 19 (2003) 3151–3156.